Acta Metall. Sin. (Engl. Lett.), 2015, **28**(4), 521–530
DOI 10.1007/s40195-015-0228-6

Anti-Corrosion and Tribo-Mechanical Properties of Co-deposited Zn–SnO_2 Composite Coating

Ojo Sunday Isaac Fayomi · Abimbola Patricia Idowu Popoola

Received: 2 June 2014 / Revised: 8 September 2014 / Published online: 17 February 2015

Abstract Zn–SnO_2 composite coatings were prepared by direct potential using electrolytic co-deposition technique from sulfate solution. The effect of Zn^{2+} and SnO_2 concentrations in deposited bath on the mechanical properties and morphological characteristics of the composite coatings were examined. The characterizations of the sample were analyzed using scanning electron microscopy couple with energy dispersive spectroscopy (SEM/EDS), X-ray diffraction (XRD) and atomic force microscopy (AFM). The electrochemical degradation behavior of the samples in 3.65 wt.% NaCl solution was studied using potentiodynamic polarization technique and characterized by high-resolution optical microscope. From all the fabricated composite coatings, obvious diffraction peaks were observed with Zn-7Sn-S-0.3V film with Zn_2Sn_7, Sn, Zn_2Sn_5 and Zn phases, confirming the presence and formation of Zn–SnO_2 coating. The XRD pattern shows that the presences of SnO_2 particle remarkably play a major role in the precipitation and orientation of the alloy matrix. From the SEM/EDS and AFM results, the deposits show that composite particle and proper bath composition have strong influence on the microstructure. An enhanced corrosion resistance was attained as a result of the induced particles.

KEY WORDS: Metal matrix composite; Co-deposition; Mechanical property; Corrosion resistance

1 Introduction

Mild steels are one of the leading engineering materials over years for many scientific and industrial applications, especially in automobile and aero-system industries, because of their unique properties [1]. Yet, their susceptibility to corrosion, poor tribological resistance and low hardness limit their applications [2, 3]. Nevertheless, many surface enhancement techniques such as thermal spray, vapor deposition, laser alloying, galvanizing and painting have been adopted to improve mild steel properties against electrochemical reaction and plastic deformation [3–7].

Co-deposition through electroplating has been found superior properties to several mentioned techniques due to their bonding characteristics [3, 8], texture, cost and thickness ratio [9–12]. Composite deposition is a trend for depositing particle of metallic and non-metallic compound in insoluble form or ceramics in electrolyte for specific functional properties [13]. Anti-corrosion and mechanical properties have been studied extensively in zinc alloy composite coatings such as Zn-Zr [14], Zn-Cr [15, 16], Zn-Co, Zn-Ni [17], Zn-TiO_2-TiAlN [18], Zn-Fe [19] prepared by different methods [20–24]. Evolution of based materials containing composite and ceramics such as TiO_2, Al_2O_3, ZnO, ZrO_2, Fe_2O_3, Cr_2O_3 and SiO_2 exhibits excellent oxidation stability and tribological resistance [25–29].

Available online at http://link.springer.com/journal/40195

O. S. I. Fayomi (✉) · A. P. I. Popoola
Department of Chemical, Metallurgical and Materials Engineering, Tshwane University of Technology, P.M.B. X680, Pretoria, South Africa
e-mail: ojosundayfayomi3@gmail.com

O. S. I. Fayomi
Department of Mechanical Engineering, Covenant University, Ota, Ogun State, Nigeria

Though, unlike other composite particles, very few on SnO_2 has been reported in open literature. Some work focused on the corrosion properties and morphological behavior of Sn-Zn coatings, but mechanical properties have not been explored [30, 31]. It is evident that for material to be used for industrial applications, corrosion behavior as well as mechanical properties should be studied [32]. In the present paper, we fabricate Zn–SnO_2 composite coatings through electrolytic deposition, microstructure of the deposited layer was characterized, and the corrosion resistance was also measured. Besides, tribological behavior was evaluated by using sliding wear test; the scanning electron microscopy with attached energy dispersive spectroscopy (SEM/EDS) was employed to characterize the morphological crystal structure/topography. The phase studies were carried out by using X-ray diffractometer (XRD) and Raman spectroscopy.

2 Experimental

2.1 Preparation of Substrates

Commercial mild steel (40 mm × 20 mm × 1 mm) sheet from Nigeria was used as the cathode, and zinc plates (60 mm × 40 mm × 2 mm) with 99.5% purity were used as the anode. The steel sheets were prepared with fine grade of emery paper as described in a previous study [23]. Samples were properly cleaned with sodium carbonate, pickled and activated with 10 wt.% HCl solution at ambient temperature for 10 s followed by instant rinsing in deionized water. The chemical composition (wt.%) of the used mild steel is: 0.15 C, 0.45 Mn, 0.18 Si, 0.01 P, 0.31 S, 0.005 Al, 0.008 Ni and balance of Fe.

2.2 Processing Details

The deposition of Zn–SnO_2 binary composite alloy was performed in a single cell containing two zinc anodes and a single cathode. The distance between the anode and the cathode is 15 mm. Before plating, analytical grade chemicals and deionized water used in solution were admixed and preheated to 40 °C. The bath solution composition is as follows: 75 g/L Zn, 10 g/L thiourea, 50 g/L $NaSO_4$, 10 g/L boric acid, 7 or 13 g/L SnO_2, 10 g/L glycine and 75 g/L $ZnSO_4$. The pH value of the bath solution is 4.8.

The chosen deposition parameter is in line with the preliminary study and the previous work [27]. The prepared electrodes were connected to the direct current via a rectifier at varying applied potential and current density between 0.3 and 0.5 V at 2 A/cm^2 for 20 min with stirring (200 r/min). The processing parameters for different samples are listed in Table 1. The distance between the anode and the cathode and the immersion depth were kept constant as described in Ref. [1]. After deposition, samples were rinsed in distilled water and air-dried thereafter sectioned for characterization.

The deposition time and voltage were varied during deposition to achieve good coating thicknesses and weight gain. The choice of each condition and parameters are optimized by our pre-study. It is expected during co-deposition micron and sub-micron grade particle inoculated into the deposition bath in either minute quantity should provide improved properties and stabilized solid structure [15]. The possibility of having a substantial coating weight and coating thickness in relation to the coating parameter is dependent on the bath formulation.

2.3 Characterization of Coating

The structure of the deposited composite coating was characterized by VEGA 3 TESCAN Scanning electron microscope (SEM) equipped with EDS. The XRD scan was performed on PANalytical Empyrean diffractometer with Pixel detector and fixed slits with Fe filtered CoK_α radiation. The phases were identified using X'Pert Highscore plus software and quantified using the Rietveld method. Micro-hardness studies were carried out by using a Diamond pyramid indenter EMCO Test Dura-scan 10 microhardness testers with a load of 0.1 N for 20 s. The average micro-hardness was measured across the plated surface in an interval of 2 cm by using screw gauge attached to the Dura hardness tester.

2.4 Friction and Wear Tests

The friction and wear behaviors of the deposited alloy were evaluated by using CERT UMT-2 muiti-functional tribological tester at ambient temperature (25 °C). The reciprocating sliding tests were carried out with a load of 5 N at a constant speed of 5 mm/s for 20 min, and the displacement amplitude is 2 mm. A Si_3N_4 ball (4 mm in diameter, 1,600 HV) was chosen as the counterpart for the evaluation of tribological behavior of the coated sample. The area of the specimen for wear tests is 2 cm × 1.5 cm. After wear tests, morphology of the wear scar and worn surface is further examined with high-magnification Nikon optical microscope.

2.5 Corrosion Studies

Corrosion resistance of the samples was evaluated by using linear potentiodynamic polarization tests. Measurements were systematically performed by using an auto-lab potentiostat (PGSTAT101 computer controlled) with the general purpose electrochemical software (NOVA 1.8)

Table 1 Processing parameters for different samples

Material sample	Time of deposition (min)	Stirring rate (r/min)	Potential (V)	Current density (A/cm^2)	SnO_2 additive (g/L)
Zn-7SnO_2-0.3V	20	200	0.3	2	7
Zn-7SnO_2-0.5V	20	200	0.5	2	7
Zn-13SnO_2-0.3V	20	200	0.3	2	13
Zn-13SnO_2-0.5V	20	200	0.5	2	13

package version. Measurements were carried out at room temperature in 3.65 wt.% NaCl solution. The NaCl solution was prepared from analytical grade reagents and distilled water. An electrochemical cell composed of working electrode (coated samples), the counter electrodes (graphite rods) and a reference electrode (Ag/AgCl 3 mol/L KCl electrode, SCE) were used. Scanning potential ranges from –1.51 V to 1.5 V with a scan rate of 1.2 V/s.

3 Results and Discussion

3.1 AFM Studies

Figures 1 and 2 show the AFM images obtained from Zn-7SnO_2-0.3V and Zn-13SnO_2-0.3V layers. There are observed structural changes in topography based on the incorporated fraction of the particulate and the deposition potential used. There was orderliness of the grain with good separation of the crystal in Zn-7SnO_2-0.3V layer. Comparing this micrograph with Zn-13SnO_2-0.3V in Fig. 2, it is observed that particles with coarse-grained formation having non-uniform crystal size. Reason for this is not clear, and it could be expected that with more of composite particles inclusion in the electrolyte, the adhesion should be instant. However, it was reported by [33] that the surface roughness increased significantly with the film thickness which was in agreement with the observation in this study where the fabricated Zn-7SnO_2-0.3V layer produced a well adhered and separated grain at moderate induced composite and lower potential rate. However, our previous observations [3, 5] revealed that metallurgical parameter for a particular alloy coating could result in unexpected crystal growth, thereby restricting the proper precipitation of particles within the cathode surface.

In all, fine-grained crystals and uniform arrangement of the distributed crystals were achieved in both coatings. Another report by [31] stated that deposition films obtained within 1.0–1.4 V mostly covered the substrate and exhibited coalesced crystallites. It is also reported that at lower potential, a fine adhesion resulted from steady throwing power could give a uniform crystal growth [1], which is in agreement with the results presented in Fig. 1.

3.2 XRD/Raman Analysis

Figures 3, 4 and 5 show the XRD patterns and Raman profile for Zn–SnO_2 sulfates deposited samples. The intermediate phase of the considered Zn–SnO_2 matrix was assessed, and all shows very similar pattern. From the profiles, possible existing phases are Zn, Zn_2Sn_7, Sn and Zn_2Sn_5 for Zn-7SnO_2-0.3V coating. The response of tin in zinc admixed bath resulted in zinc-tin intermetallic precipitates. Generally, the coating consists of peak with

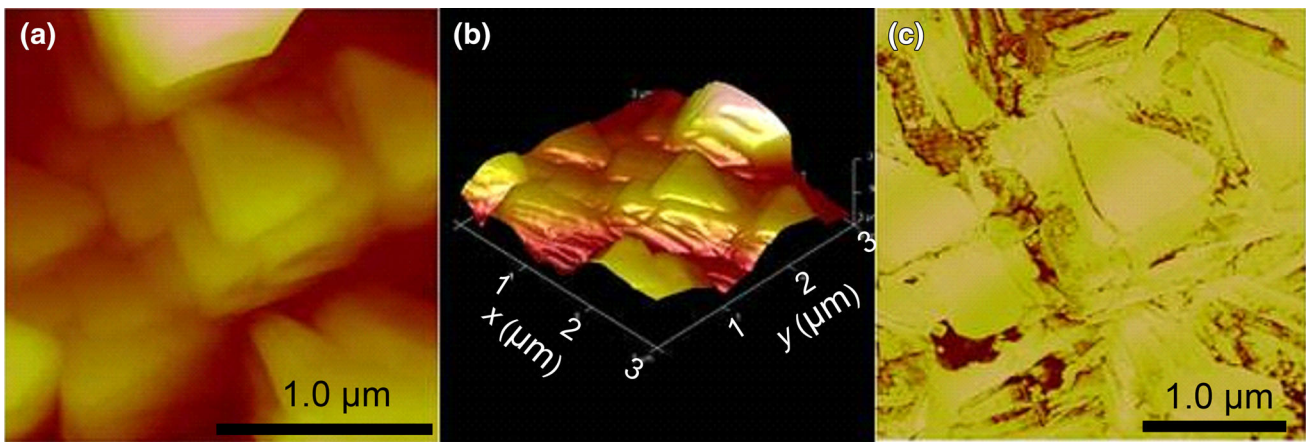

Fig. 1 AFM images of the Zn-7SnO_2-0.3 V layer: **a** 2D image; **b** 3D relief image; **c** roughness analysis

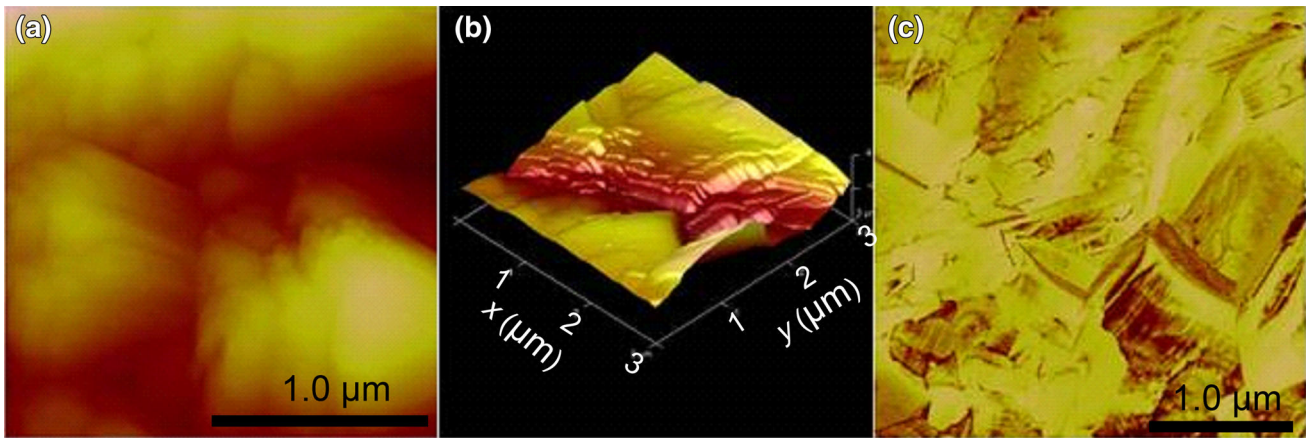

Fig. 2 AFM images of the Zn-13SnO_2-0.3V layer: **a** 2D image; **b** 3D relief image; **c** roughness analysis

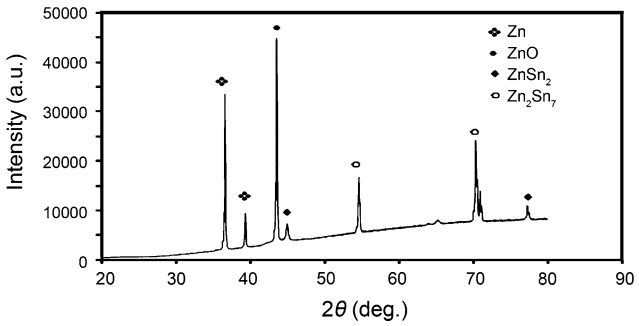

Fig. 3 XRD pattern for Zn-7SnO_2-0.3V coating

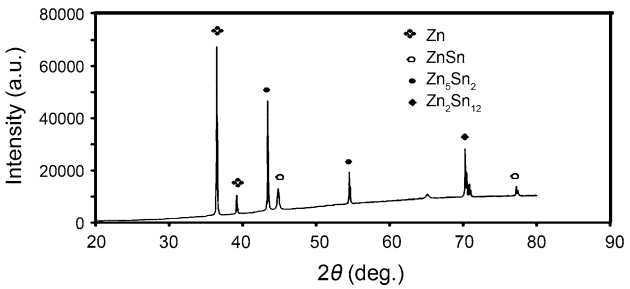

Fig. 4 XRD pattern for Zn-13SnO_2-0.5V coating

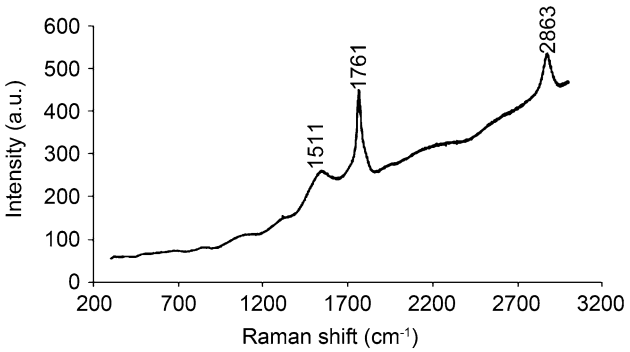

Fig. 5 Raman spectrum for Zn-7SnO_2-0.3V coating

strong plane and Zn-7SnO_2-0.3V produced a better phase as a result of smaller crystal. It is reported that current densities often influence the produced grain size, which could determine the phase composition of such coating [19, 34]. Considering the decreased sulfur in bath due to Zn^{2+} and Sn^{2+}cation, the visibility of the plane is a function of dissolution of sulfur, which leads to the improvement in crystallinity of the deposits. However, when comparing Zn-13SnO_2-0.5V to Zn-7 SnO_2-0.3V, the significant differences were found to be peak level as a result of the bonding effect. The similarities in XRD patterns confirmed the presence of composite particle, while the differences in the peaks could be attributed to the rate of deposition. Zn_2Sn_7, ZnSn and Zn account for the major peaks for Zn-13SnO_2-0.5V binary composite coating as presented in Fig. 4.

The effect of SnO_2 incorporated composite particle in the electrolyte of Zn-7SnO_2-0.3V matrix was examined by Raman spectrum. As shown in Fig. 5, a remarkable shift was observed at 2,863 cm^{-1}, in accordance with the result obtained from XRD pattern. The predominate intensity of about 500 a.u. was noted for the Zn-7SnO_2-0.3V, which is the best among the deposited series. It should be mentioned that the adsorption of Sn by Zn^{2+} is responsible for the shield growth of the intensities. It is believed that the incorporation of composite particle will shift diffraction pattern [16].

3.3 SEM/EDS Results

SEM/EDS results on the influence of composites particle incorporated in the Zn–SnO_2 matrix are shown in Figs. 6 and 7. The structure comprises of dispatched shape crystallites of various compactable sizes. Moreover, the particles are more adhered with Zn-7SnO_2-0.3V matrix. Grains show a different shape from Zn-13SnO_2-0.5V coating as expected. Although study by [12] affirmed that the grain

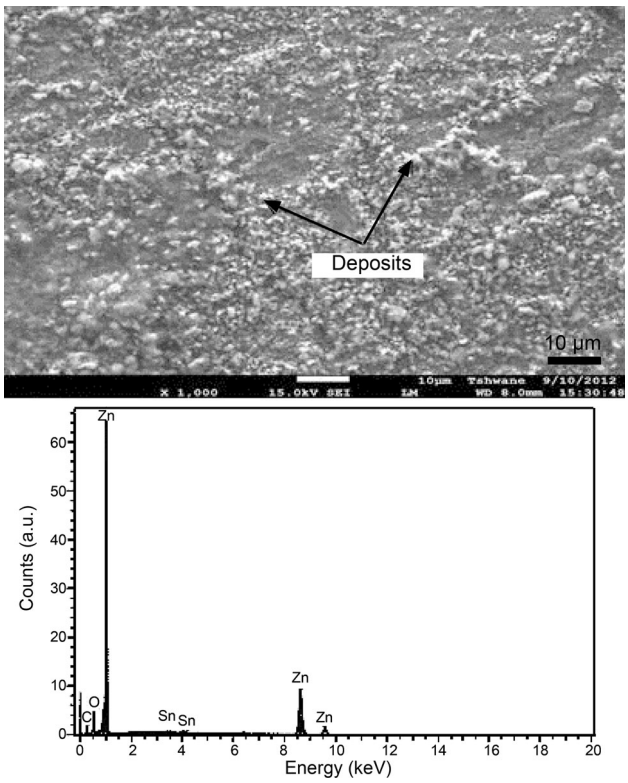

Fig. 6 SEM image and EDS result of Zn-7SnO_2-0.3V coating

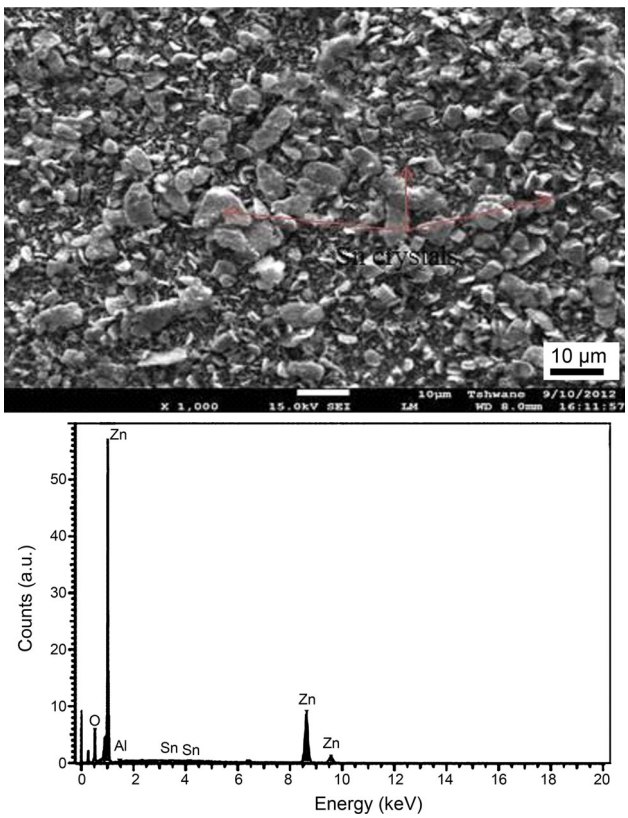

Fig. 7 SEM image and EDS result of Zn-13SnO_2-0.5V coating

size of a metallic matrix is independent on the composite concentration, which is in correlation to our findings. Although slight increase is observed on the grain size of the matrixes prepared with higher incorporated particle. This stable adhesion is supported by report made by [31].

On the contrary, the observation on this regard might not be fully agreed with each other in all the deposition studies, and the reason might be that particle embedded in the coatings could influence the orientation of the metallic coatings matrix which could also affect the grain size. More so, composite particle has strong effect on the deposited surface structure, and the changes in deposition mechanism should be the main reason for morphology differences. The nucleation and the crystal growth could be attributed to the current density and potential, which is in agreement with previous reported result of [34]. No pores were observed on the surface of the Zn-7SnO_2-0.3V. The EDS identified the presence of Sn ions distributed within the Zn interface. Distinctive larger crystals were observed in Zn-13SnO_2-0.5V coating compared to Zn-7SnO_2-0.3V.

If the deposition rate is faster due to higher applied potential, alloy deposits have a large number of tiny particles on the cathode's surface that could produce irregular cluster of crystal as indicated in Fig. 7.

Figure 8 shows the optical micrographs of the binary fabricated Zn-7SnO_2-0.3V matrix and composite coating produced at Zn-13SnO_2-0.5V, respectively. There is smaller crystal nucleus for Zn-7SnO_2-0.3V than that for Zn-13SnO_2-0.5V, which is in accordance with SEM observations. The nature of the deposit is uniform and adherent except some few overlaps in the region. The morphological of Zn-7SnO_2-0.3V in Fig. 8a mostly exhibits small and compact deposit without porosity on the interface. For Zn-13SnO_2-0.5V (Fig. 8b) composite coating, dark region within the surfaces was observed, which may actually be caused by the difference in process parameters.

3.4 Micro-Hardness Tests

The micro-hardness of the deposited coatings for each sample at different applied potentials was compared with the measured mild steel as-received sample as shown in Fig. 9. It can be seen that the hardness increased from 33.5 HV for base mild steel to approximately 116 HV for the hardest composite alloy. It is observed that increase in composite content from 7 to 13 g/L did significantly change the hardness characteristics. The incorporation of SnO_2 improved the micro-hardness to some appreciable point with Zn-7SnO_2-0.3V alloy possessing the highest hardness of 116 HV.

The micro-hardness of the best improved coating doubles the substrate value. Reason for this improvement is

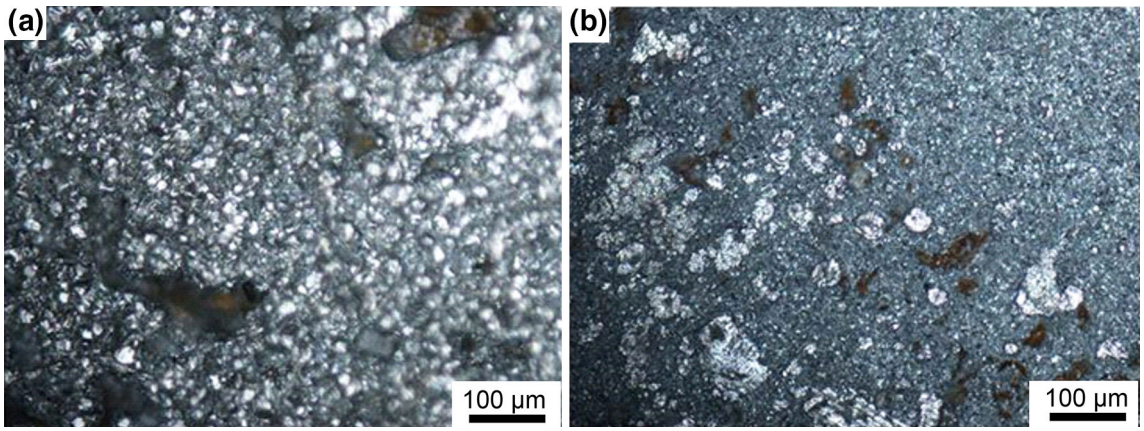

Fig. 8 SEM images of Zn-7SnO_2-0.3V **a**, Zn-13SnO_2-0.5V **b**

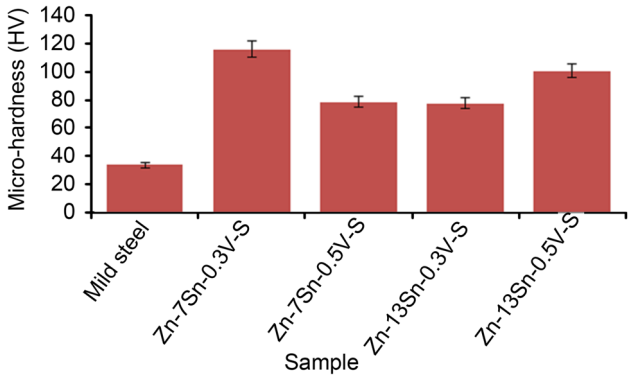

Fig. 9 Micro-hardness for Zn–SnO_2 composite coatings

numerous: firstly, the in situ intermetallic phase could result into the improved hardness observed. Moreover, at lower current density and potential, the longer deposition time required to give a preferred thickness [16] forces the particle to precipitate at the cathode, which hence changes the structural properties. Therefore, the possibility of agglomeration and entrapment of the particle at the cathode could result in an improved hardness coating. On the other hand, microstructure characteristics of individual materials and the atomic bonding could also result in improved hardness propagation. However, [28, 31] reported that the higher hardness of the coating is often caused by the fine-grained structure of the deposit or alloys and the dispersed particles in the fine-grained matrix. Contrary to the obtained results of Zn-13SnO_2-0.5V coating with 100.6 HVN, it is obvious that increasing the deposition rate and composite incorporation does not facilitate thin film dispersion into the Zn-matrix. These results were ascertained by [24, 33] report that higher amount of particle incorporation is not directly correlated with crystallite, and the crystalline size is dependent on the variety of additional plating parameter.

3.5 Wear Behavior

Figure 10 shows the wear loss of the substrate and the deposited alloy. All the composites' admixed deposited coating exhibits lower wear loss. The wear loss for the as-received sample is about 2.351 g/min, while the Zn-7SnO_2-0.3V coating has the lowest wear rate of 0.005 g/min. It is believed that composite particles migrated from the bath through the influence of applied potential in the cathodic region significantly provide a cohesive structural effect needed for improved properties as observed for all coated alloys. More so, it is certain that SnO_2 particles co-deposited in the Zn-matrix could restrain grain growth of zinc and hence influence by reducing the occurrence of plastic deformation under applied force. It is reported that SnO_2 contents strengthen mechanical properties and thus provide a suitable wear resistance [36].

Figures 11 and 12 present the friction coefficient against time and sliding velocity of the as-deposited Zn-7SnO_2-0.3V composite coating and mild steel substrate. The substrate had the highest friction coefficient in the tested duration and under all velocities. On the contrary, as-deposited composite alloy had lower friction. The lower coefficient could be attributed to the coherent precipitation of

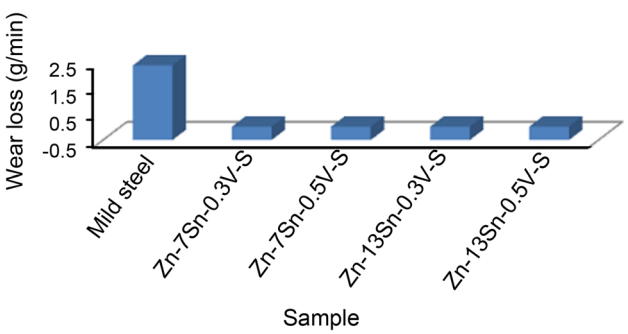

Fig. 10 Wear rate of mild steel and Zn-Sn-S coatings

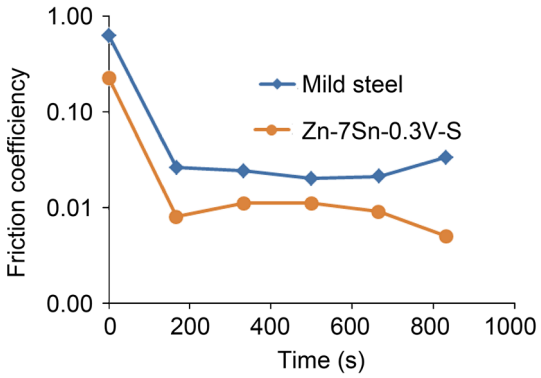

Fig. 11 Variation of friction co-efficient against time for Zn-7SnO_2-0.3V coating and the mild steel substrate

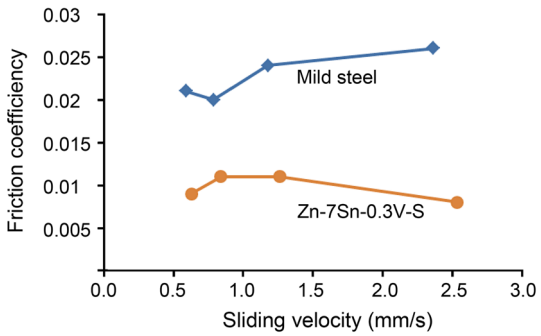

Fig. 12 Variation of friction co-efficient against sliding velocity for Zn-7SnO_2-0.3V coating and mild steel substrate

SnO_2 to demonstrate friction-reducing behavior in the Zn-Sn matrix at lower potential. Similar result has also been reported by [17]. It is important to mention that since incorporation of SnO_2 particle could alter the microstructure and strengthen the coatings, the compact and crack-free coating may also assist in the minimal friction coefficient.

Figure 13 shows the morphology of the worn surface of the mild steel substrate. Obviously, plastic deformation, grooves, pits and fracture were observed on the surface of the substrate.

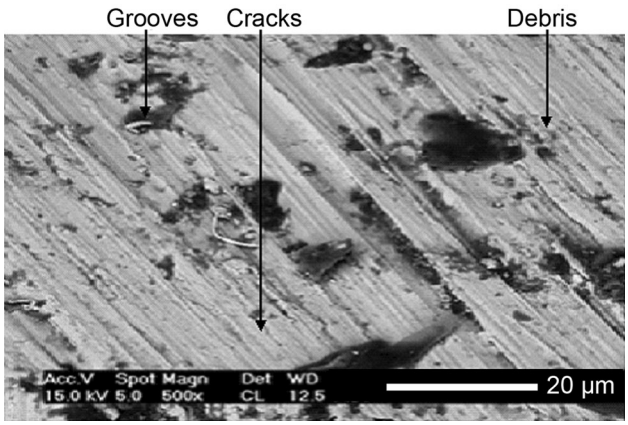

Fig. 13 SEM image of the wear scar of the mild steel substrate

Figure 14 shows the morphologies of the worn surfaces of the Zn-7SnO_2-0.5V and Zn-13SnO_2-0.5V coatings. From Fig. 14, it can be found that few fractures with mild damage are observed on the worn surfaces of composite coatings. Noticeably the deposits possess very smooth worn surfaces. For Zn-13SnO_2-0.5V coating, plastic deformation seems more visible due to wear product or weak adhesion (Fig. 14b). The formation of oxide films on the wear surface is often seen to provide a significant wear resistance [35]. The zinc–tin binary alloys have a multi-phase structure and ions consisting of mainly tin-rich and zinc-rich phases. In addition, oxide films are formed on the surface of zinc–tin alloys during reciprocating sliding, which contribute to their excellent wear resistance. It should be noted that stable adhesion gives good structural properties [18], and this, however, could give better wear flow than the visible irregular degradation and fracture on the as-received sample.

3.6 Corrosion Resistance of Zn–SnO_2 Coatings

The electrochemical behavior of the Zn–SnO_2 coatings was examined using a linear potentiodynamic polarization. For quantitative studies, the immersion was performed in 3.65 wt.% NaCl and the polarization curve is presented in Fig. 15. The potential of the as-deposited composite alloy was observed to shift toward positive values for all the samples, while the substrate moves drastically toward more negative region. The negative shift of the potential shows strong dissolution of the mild steel films due to the absence of surface protection [23]. The positive shift of the potential indicates the formation of protective film and an increase in the passive film thickness. Among the composite deposited coatings, Zn-7SnO_2-0.3V obtained a more stable passivity than the other coatings due to the large number of tiny particles deposited on the cathode surface at higher applied voltage.

Moreover, it was also observed that the corrosion rate decreases obviously with the presence of Zn–SnO_2 coatings. The composite particle improved corrosion resistance, which is against the viewpoint in [9] that the microstructure of the deposited coating has less effect on corrosion resistance. Practically, the effects of ions in composite particle include blocking the actives sites and modify the structure, which could shift passivation toward positive region. With this, there is a decrease in current density, which could also lead to a decrease in corrosion rate and hence provide high E_{corr}.

The results of polarization measurements for the investigated specimens are summarized in Table 2. Obviously, the buildup of strong adhesive and the corrosion

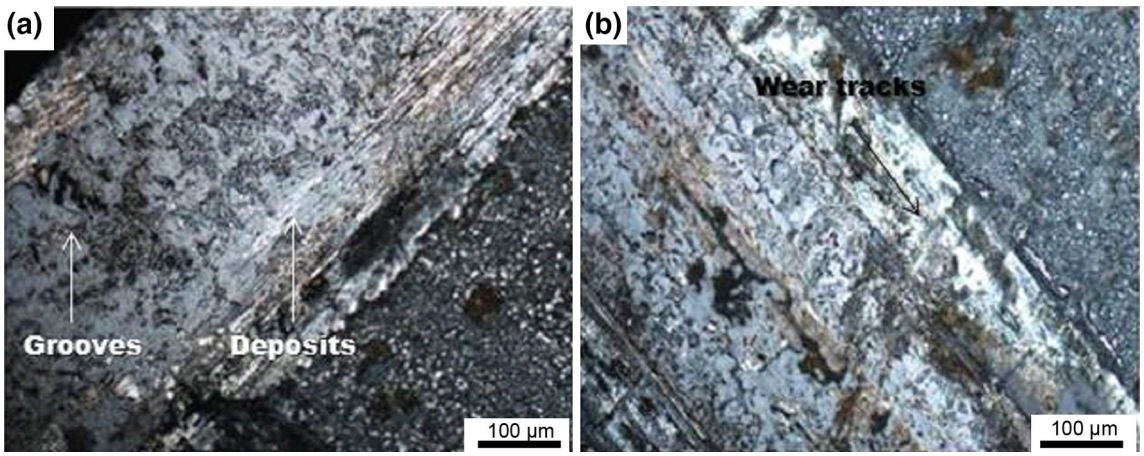

Fig. 14 Micrographs of the wear scars of Zn-7SnO_2-0.5V **a**, Zn-13SnO_2-0.5V **b** coatings

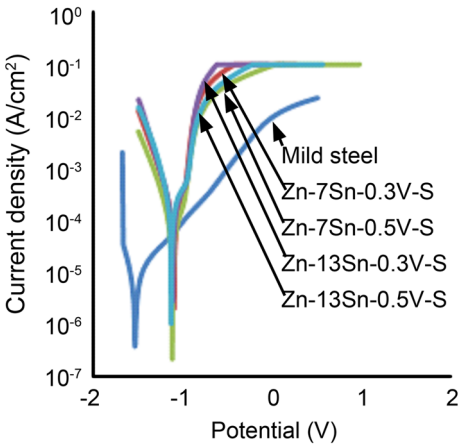

Fig. 15 Potentiodynamic polarization curves for Zn–SnO_2 coatings and mild steel

potential observed from these samples is dependent on alloy composition and composites content. The corrosion potential of as-deposited samples for Zn-7SnO_2-0.3V is −1.09955 V, while that of mild steel is −1.539 V, which implies that corrosion potential increased by 0.44 V. Furthermore, composite coating displayed reduced corrosion current density in all instances as compared to the mild steel. From the polarization results, mild steel exhibited highest corrosion current density (i_{corr}) of (7.04×10^{-2} A/cm^2) among all the as-deposited samples, while Zn-7SnO_2-0.3 V had the i_{corr} of 1.87×10^{-5} A/cm^2, and a three-order magnitude decrease in corrosion current density was attained due to the effects of alloy composition electrodeposited on mild steel. Polarization resistance (R_p) for Zn-7SnO_2-0.3V is 5.64×10^3 Ω that was the highest for all coated samples on this matrix. Three-order increase in magnitude was attained when compared to 2.76×10^2 Ω for the as-received sample. At this point, it is noteworthy to mention that corrosion resistance of the substrate is enhanced drastically with the addition of tin inclusion at the deposits rather than Zn film alone because co-deposition of this binary alloy formation is a function of passive film containing Sn^{2+} and Zn^{2+}, which are active barriers against corrosion degradation.

Qualitative studies of the sample surface after corrosion test were examined by AFM as shown in Fig. 16 and OM illustrated in Fig. 17a, respectively, for Zn-7SnO_2-0.3V coating. After corrosion, white oxide film formed on the coating surface. The degree of irregularities and surface imperfection were very minimal. Such is expected in

Table 2 Summary of the potentiodynamic polarization results of Zn–SnO_2 coating and mild steel

Sample	I_{corr} (A)	i_{corr} (A/cm^2)	R_P (Ω)	E_{corr} (V)	V_{corr} (mm/year)
Mild steel	2.04×10^{-3}	7.04×10^{-2}	27.600	−1.53900	4.1
Zn-7SnO_2-0.3V	1.87×10^{-5}	1.87×10^{-5}	564.93	−1.09955	0.007786
Zn-7SnO_2-0.5V	1.92×10^{-5}	1.92×10^{-5}	446.02	−1.12122	0.007995
Zn-13SnO_2-0.3V	2.17×10^{-5}	2.17×10^{-5}	406.13	−1.11633	0.009060
Zn-13SnO_2-0.5V	5.44×10^{-5}	5.44×10^{-5}	77.653	−1.13342	0.022678

I_{corr} is the corrosion current, i_{corr} is the corrosion current density, R_p is the polarization resistance, E_{corr} is the corrosion potential, V_{corr} is the corrosion rate

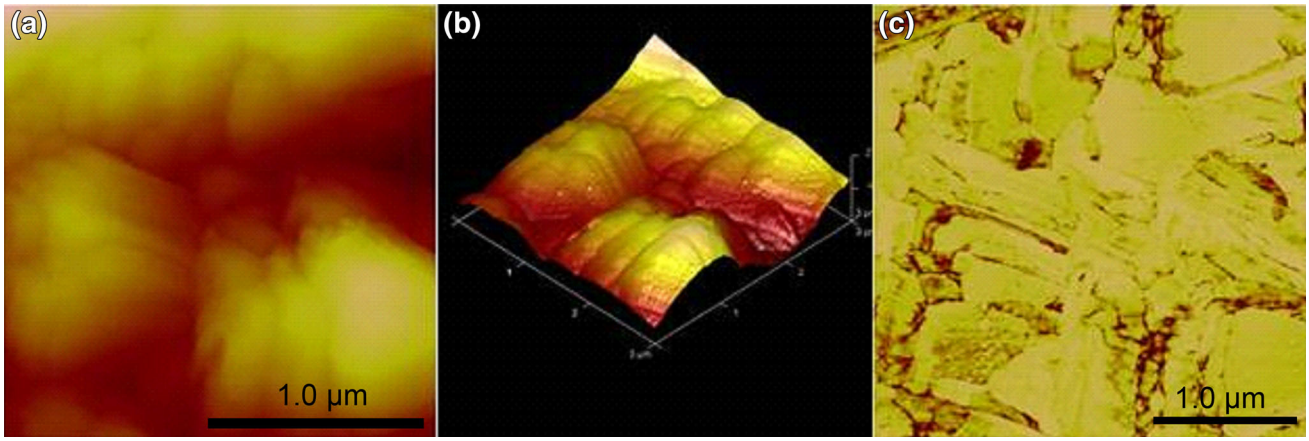

Fig. 16 AFM images of the Zn-7SnO_2-0.3V coating surface after corrosion: **a** 2D image; **b** 3D relief image; **c** roughness analysis

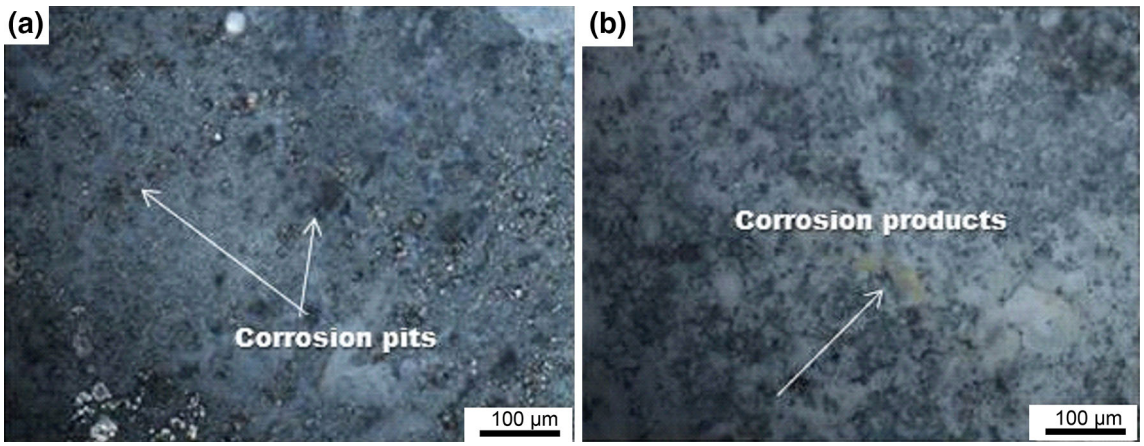

Fig. 17 Morphologies of corroded surface of Zn-7SnO_2-0.3V **a**, Zn-13SnO_2-0.5V **b** coatings

binary co-deposition system if little porosity is obtained from microstructural properties. It was pointed out that the morphological characteristics of deposited coating depend on the applied voltage, bath composition and the additives [9]. It was reported that since the deposition rate is slow at low applied voltage at the beginning of the electrolysis, alloy deposits have a large number of tiny particles on almost all over the cathode surface, which acts as nucleation for further deposition at the preferential sites [6].

Popoola et al. [28] pointed out that the range of passivation is a condition existing on a metal surface, because of the presence of a protective film that markedly lowers the rate of corrosion process. All these evidences by various authors are in agreement with present results that chloride ion could not affect the structural modification due to strong precipitation and reinforcement of coated alloy.

However, after corrosion, very little visible degradation could be observed on the surface of the deposited Zn-13SnO_2-0.5V coating (see Fig. 17b). This can be attributed to the increase in the nucleation and growth exhibited by the admixed particles. Enhanced contribution and uniform distribution of SnO_2 favors oxidation stability of the coated alloys.

4 Conclusions

1. Bright and cohesive Zn–SnO_2 coatings were fabricated using co-deposition method. Adding a small amount of SnO_2 particles into the sulfate bath can improve the microstructure property of the Zn–SnO_2 coating. The Sn ions dissolve homogeneously and further increase the oxidation resistance of the Zn–SnO_2 scale.
2. The wear resistance of the deposited coating increased compared with that of the mild steel. The friction coefficients of the all coatings were lower than those of mild steel as a result of incorporated particle.
3. The corrosion resistance of mild steel was significantly improved after Zn–SnO_2 deposition. The increase in corrosion resistance of the entire composite coating is

attributed to the formation of high Sn-containing alloy phase.

Acknowledgments This material is based upon the work supported financially by National Research Foundation and Surface Engineering Research Centre, Tshwane University of Technology, Pretoria, South Africa.

References

[1] O.S.I. Fayomi, A.P.I. Popoola, Res. Chem. Intermediate. **39**, 1313 (2013)
[2] C.M. Kumar, K. Kumar, T.V. Venkatesha, K. Vathsala, K.O. Nayana, J. Coat. Technol. Res. **9**, 71 (2012)
[3] A.P.I. Popoola, O.S.I. Fayomi, Int. J. Electron. Sci. **6**, 3254 (2011)
[4] B.M. Praveen, T.V. Venkatesha, Appl. Surf. Sci. **254**, 2418 (2008)
[5] C.C. Lin, C.M. Huang, J. Coat. Technol. Res. **3**, 99 (2006)
[6] R. Xu, J. Wang, Z. Guo, H. Wang, J. Rare Earth **26**, 579 (2008)
[7] O. Sancakoglu, O. Culha, M. Toparli, B. Agaday, E. Celik, Mater. Des. **32**, 4054 (2011)
[8] G. Yang, S. Chai, X. Xiong, S. Zhang, L. Yu, P. Zhang, Trans. Nonferrous Met. Soc. China **22**, 366 (2012)
[9] M.J. Rahman, S.R. Sen, M. Moniruzzaman, K.M. Shorowordi, J. Mech. Eng. Trans. **40**, 9 (2009)
[10] C.M. Kumar, P. Kumar, T.V. Venkatesha, K. Vathsala, K.O. Nayana, J. Coat. Technol. Res. **151**, 9 (2012)
[11] M. Arici, H. Nazir, A. Aksu, J. Alloys Compd. **509**, 1534 (2011)
[12] J. Fustes, A. Gomes, M.I. Silva, Pereira. J. Solid State Electrochem. **121**, 1435 (2008)
[13] T.G. Wang, D. Jeong, Y. Liu, S. Lyengar, S. Melin, K.H. Kim, Surf. Coat. Technol. **206**, 2638 (2012)
[14] S.M.A. Shibli, F. Chacko, C. Divya, Corros. Sci. **52**, 518 (2010)
[15] A. Gomes, T. Frade, I.D. Nogueira, J. Sci. Technol. **2**, 1146 (2012)
[16] M. Srivastava, J.N. Balaraju, B. Ravishankar, K.S. Rajam, Surf. Coat. Technol. **205**, 66 (2010)
[17] D. Dong, X.H. Chen, W.T. Xiao, G.B. Yang, P.Y. Zhang, Appl. Surf. Sci. **255**, 7051 (2009)
[18] J.L. Mo, M.H. Zhu, B. Lei, Y.X. Leng, N. Huang, Wear **263**, 1423 (2007)
[19] M.M. Abou-Krisha, F.H. Assaf, S.A.J. El-Naby, J. Coat. Technol. Res. **6**, 391 (2009)
[20] B. Subramanian, S. Mohan, S. Jayakrishnan, Surf. Coat. Technol. **201**, 1145 (2006)
[21] K.H. Zum Gahr, Wear **200**, 215 (1996)
[22] C.K. Lee, Tribol. Int. **55**, 7 (2012)
[23] A.P.I. Popoola, O.S.I. Fayomi, O.M. Popoola, Int. J. Electrochem. Sci. **7**, 4898 (2012)
[24] T. Frade, Z. Bouzon, A. Gomes, M.I. Da Silva, Surf. Coat. Technol. **204**, 3592 (2010)
[25] W. Zhang, W. Liu, C. Wang. J. Eur. Ceramic. Soc. 7, 2869 (2002)
[26] A. Abdel, M.A. Barakat, R.M. Mohamed, Appl. Surf. **254**, 4577 (2008)
[27] O.S.I. Fayomi, M. Abdulwahab, A.P.I. Popoola, J. Ovonic Res. **9**, 123 (2013)
[28] A.P.I. Popoola, O.S.I. Fayomi, O.M. Popoola, Int. J. Electrochem. Sci. **7**, 4898 (2012)
[29] H. Kazimierezak, P. Ozga, Surf. Sci. **607**, 33 (2013)
[30] Z. Dong, X. Peng, Y. Guan, L. Li, F. Wang, Corros. Sci. **62**, 147 (2012)
[31] G.A. Finazzi, E.M. Oliveira, I.A. Carlos, Surf. Coat. Technol. **9**, 187 (2004)
[32] T. Dikici, O. Culha, M. Toparli, J. Coat. Technol. Res. **7**, 792 (2010)
[33] A.A. Volinsky, J. Vella, I.S. Adhihetty, V.L. Sarihan, L. Mercado, B.H. Yeung, W.W. Gerberich, Mater. Res. Soc. **649**, 1 (2001)
[34] D.E. Rusu, A. Ispas, A. Bund, C. Gheorghies, G. Cârâc, J. Coat. Technol. Res. **9**, 1 (2012)
[35] P. Gençğga, S.S. Temel, K. Tevfik, M. Samuel, Wear **8**, 94 (2002)
[36] B.K. Prasad, Wear **240**, 100 (2000)